Drivers of the Mixed Layer Salinity Seasonal Variability in the Arctic Ocean

Alexandre Supply[1], Camille Lique[1], Nicolas Kolodziejczyk[1], Claude Talandier[1]

[1] Univ. Brest, CNRS, IRD, Ifremer, Laboratoire d'Océanographie Physique et Spatiale (LOPS), IUEM, Brest 29280, France.

Corresponding author: Alexandre Supply (alexandre.supply@univ-brest.fr)

Key points

- Arctic mixed layer salinity seasonality is driven by a 1D balance between sea ice freshwater flux, mixing and entrainment at its base.
- On the shelves, the horizontal advection of freshwater from the river runoff modulates significantly the 1D balance.
- The largest variations are found within 100km of the sea ice edge, where all the processes at play are intensified.

Abstract

The processes driving the seasonal variability of the mixed layer salinity in the Arctic Ocean are investigated using a simulation performed with regional ocean – sea ice model at high resolution. While the seasonal variations of the mixed layer depth remain small, in particular under the perennial sea ice (O(30m)), the mean salinity of the mixed layer varies largely, with a seasonal cycle as high as 3 pss. On the shelves, where the sea ice is seasonal, the mixed layer is much fresher but exhibits a seasonal cycle with a similar amplitude. Overall, the seasonal variability of the mixed layer salinity results largely from a 1D vertical balance between the freshwater flux at the surface arising from the sea ice melt and freezing processes, and vertical mixing and entrainment occurring at the base of the mixed layer. The largest variations are found in summer, when the mixed layer is the thinnest. Over the shelves, this simple 1D balance is complexified due to the role of advection and river runoff that can locally affect the mixed layer depth and salinity. Interestingly, the largest variations are found less than 100km on each side of the sea ice edge, where all the processes affecting the mixed layer are amplified. This suggests the need to better observed and understand the ocean-sea ice-atmosphere exchanges in these regions.

Plain language summary

In this study, we use results of a numerical model run at high resolution to examine the seasonal cycle of the ocean surface conditions in the Arctic basin. In the ice-covered Arctic, the seasonal variations of the salinity of the surface layer are largely driven by the freezing and

melting cycle of sea ice, and modulated by the changes of mixed layer depth that tend to mix and entrain saltier waters found below the mixed layer. Additionally, the advection of fresh water, resulting largely from the local freshwater inputs from the rivers along the coast, can modulate the salinity of the mixed layer. We find an amplified seasonality of the mixed layer depth and salinity less than 100km on each side of the sea ice edge, suggesting a need to better monitor these regions where observations are currently particularly sparse.

Keywords

Arctic Ocean; Mixed Layer; Salinity; Seasonal Ice Zone; Sea Ice Edge.

1 Introduction

In the Arctic Ocean, the temporal and spatial variations of salinity determine the upper the density and stratification (Carmack, 2007; Johnson et al., 2012; Stewart and Haine, 2016). Such a salinity-driven stratification is characteristic of the polar regions and is required for sea ice to form (Carmack, 2007). Another well-known characteristic of the Arctic region is indeed the presence of sea ice, which has drastically declined of the past decades in response to the on-going climate change. Indeed, since 2003, the Arctic Ocean has lost one third of its winter sea ice volume, due to the decrease in coverage and the thinning of the multiyear ice (Kwok, 2018; Kacimi and Kwok, 2022), so that the Arctic is entering a seasonal sea ice regime associated with an intensified water cycle (Kinnard et al., 2008; Haine and Martin, 2017), also associated with an intensification of melting and freezing phases. These changes are particularly pronounced on the Arctic shelves (Stroeve and Notz, 2018; Arthun et al., 2021). We anticipate that the first effects of the changes in sea ice condition will be seen on the seasonal cycle of the Arctic Ocean mixed layer salinity (MLS) that is largely driven by the seasonality in sea ice.

Peralta-Ferriz and Woodgate (2015) have performed a comprehensive description of the Arctic Ocean mixed layer temporal and spatial variability using all available in-situ measurements. They have reported that the successive phases of sea ice melt and freezing induce a strong variability in mixed layer salinity and depth. During spring and summer, sea ice melt freshens and stratifies surface waters, resulting in a shoaling of the mixed layer. The mixed layer

depth (MLD) remains shallow as long as sea ice persists and limits wind-driven mixing. During winter, brine rejection salinizes the surface layer, inducing convection that drives a deepening of the mixed layer (Lemke and Manley, 1984; Toole et al., 2010). Overall, the Arctic Ocean MLD exhibits a large spatial variability. It can be particularly shallow, with records shallower than 10 meters in the Beaufort Sea and Canadian Basin during summer, while it reaches 170 m on average in the ice-free parts of the Barents Sea (Peralta-Ferriz and Woodgate, 2015).

In the Arctic Ocean, because of the peculiar stratification, heat can be stored within the mixed layer (the amount is then depending on the ice-free period duration; Stroeve et al., 2014) or just below the mixed layer, forming a near-surface temperature maximum whose heat can be stored for a winter and brought back to the mixed layer (Steele et al., 2011; Jackson et al., 2012; Timmermans, 2015; Smith et al., 2018), possibly modulating sea ice formation (Kawaguchi et al., 2014).

In addition to its large seasonality, the Arctic surface salinity also presents large spatial variations. At the Arctic gateways, warm and salty water from the Atlantic enter the Arctic through Fram Strait and the Barents Sea, while relatively fresh water from the Pacific enters through Bering Strait and the Chukchi Sea. Observations have revealed an increase of the volume of water coming from the Pacific and the Atlantic over the past 30 years, under a process named borealization (Polyakov et al. 2020). This process is associated with a weakening of the cold halocline that favors convection of warm Atlantic water during winter sea ice formation (Polyakov et al., 2020). In addition to the melting/freezing processes, the atmospheric forcing also strongly affects the Arctic Ocean mixed layer dynamics as it transfers momentum to the ocean, potentially modulated by the presence of sea ice (Rainville et al. 2011).

Although 1D vertical processes may provide a robust first order dynamical balance of the mixed layer in most of the Arctic (Peralta-Ferriz and Woodgate, 2015; Dewey et al, 2017), this balance does not provide a complete understanding of mixed layer variability (Toole et al., 2010). Lateral processes, such as meltwater advection or dense water flowing under lighter water, may induce restratification from submesoscales to regional scales (Timmermans et al., 2012; Crews et al., 2022) and complexify the interpretation of MLS variability. Moreover, previous studies have revealed the strong submesoscale dynamics in the vicinity of the sea ice edge, enhanced by the mixed layer instabilities induced by meltwater fronts (Manucharyan et al.,

2017). The wind may also drive some spatial variations of the mixed layer properties by advecting of the river plume through Ekman transport (Macdonald et al.; 1999; Mulligan and Perrie, 2019; Tarasenko et al., 2021). More generally, over the Eurasian shelves, numerous river plumes provide a large amount of freshwater, enhancing the mixed layer stratification and leading to the important mixed layer variability (Janout et al., 2016).

The diversity of the processes driving the Arctic Ocean mixed layer variability is expected to be regionally and seasonally dependent. Nevertheless, the relative contributions of the different processes influencing the MLS budget and their regional dependency remain poorly documented at the Arctic basin scale. It is also the case for the specific role of the region close to the sea ice edge (SIE) on the mixed layer. In this study, we analyze a simulation performed with a regional Arctic-North Atlantic high-resolution model to quantify the MLS budget and examine its spatial and seasonal variability. The simulation and methods used to conduct our investigations are presented in Section 2. The temporal and spatial variability of the Arctic mixed layer properties are quantified in section 3. A full seasonal MLS budget is estimated in Section 4, and then we zoom on the different terms of the budget in the region close to the SIE in Section 5. Conclusions and discussions are given in Section 6.

2 Data and Methods

2.1 Model Configuration

Our analysis relies on the use of the regional Arctic-North Atlantic high-resolution model configuration named CREG12 (Canadian REGional, Dupont et al. 2015). It is based on the NEMO 3.6 (Madec, 2016) and LIM 3.5 (Rousset et al. 2015) numerical models for the ocean and sea ice components, respectively. The configuration covers the Arctic Basin and part of the North Atlantic (down to 27°N). It has a high vertical (75 levels, with 10 levels within the top 14m of the water column) and horizontal (3–4km) resolution in the Arctic Ocean, meaning that baroclinic eddies are resolved everywhere in the Arctic except on the shallow shelves (Regan et al, 2020; Meneghello et al, 2021).

Initial conditions are taken from the World Ocean Atlas 2009 climatology for temperature and salinity while the ocean is at rest. The initial sea ice thickness and concentration

are taken from a long global ORCA12 simulation performed by the Drakkar group (Tréguier et al. 2014). Along the lateral open boundaries, monthly mean condition (comprising 3D velocities, temperature and salinity, and sea ice thickness and concentration) taken from the same ORCA12 simulation are applied. Through the Bering Strait, the transports of volume, heat and freshwater closely resemble the observational estimates from Woodgate (2018). Regarding atmospheric forcing, we use the latest version of the Drakkar Forcing Set (DFS 5.2, which is an updated version of the forcing set described in Brodeau et al. 2010). Input from the river and ice sheet runoff has been recently corrected to include the large and increasing contribution from Greenland (Hu et al. 2019).

The run of the simulations used in this study covers the period from 1979 to 2015 and is described in further details by Talandier and Lique (2021). Extended evaluation of the ocean and sea ice conditions in the Arctic Basin can be found in Regan et al. (2020) and Barton et al. (2022). Here we focus on the period after 1994 to allow for an initial spin up of the ocean and sea ice conditions. Our analysis is done based on the 5 day-average outputs.

2.2 Mixed Layer Budget

In this study, we defined the mixed layer depth (MLD; unit: m) using a 0.1 kg.m^{-3} density threshold, following Peralta-Ferriz and Woodgate (2015). The MLS budget is diagnosed as (following Moisan and Niiler (1998), Kolodziejczyk and Gaillard (2013) and Pellichero et al (2017)):

$$\partial_t S = \frac{S\,F_{surf}}{\rho\,H} - \vec{u}.\nabla S + A_h \Delta^2 S + \kappa_T \partial_z S + \frac{\Delta S}{H}(\partial_t H + \nabla H.\overrightarrow{u_H} + w_H) \qquad (1)$$

With H the MLD, S the salinity, ρ the potential density and u the velocity, all three averaged within the mixed layer, $\overrightarrow{u_H}$ and w_H the velocity at the base of the mixed layer, A_h the coefficient of horizontal mixing (or diffusivity), ΔS is the vertical gradient of salinity at the base of the mixed layer, usually define as the difference between the salinity at the base of the mixed layer and the salinity 15m below the mixed layer (Ren et al., 2011; Pellichero et al., 2017), w is the vertical velocity at the base of the mixed layer and κ_z the vertical eddy diffusivity for salinity.

The left-hand term is the MLS tendency. The first right hand term corresponds to the surface flux:

$$\frac{S\,F_{surf}}{\rho\,H} = \frac{S}{\rho\,H}(F_{ice.} + E - P + R) \qquad (2)$$

where F_{surf} are the total surface freshwater surface flux which is the sum of the flux induced by the melting and freezing of sea ice (F_{ice}), E is evaporation, P is precipitation (both rain and snow), and R is the river runoff and evaporation minus precipitation. The second and third right hand term correspond to the vertical processes and is the sum of the horizontal advection within the mixed layer and the horizontal diffusion. The last two right hand term correspond to the vertical processes, that are the vertical diffusion and the entrainment. Entrainment is only considered when the entrainment velocity $w_e = (\partial_t H + \nabla H . u_H + w_H)$ is positive as an outgoing flow at the base of the mixed layer with the same salinity than the mixed layer will not induce any change in MLS.

We estimate the MLS budget for each grid point of the model domain using the 5-days means, and then consider four regions that represent the diversity of conditions encountered over the Arctic Ocean (Figure 1a).

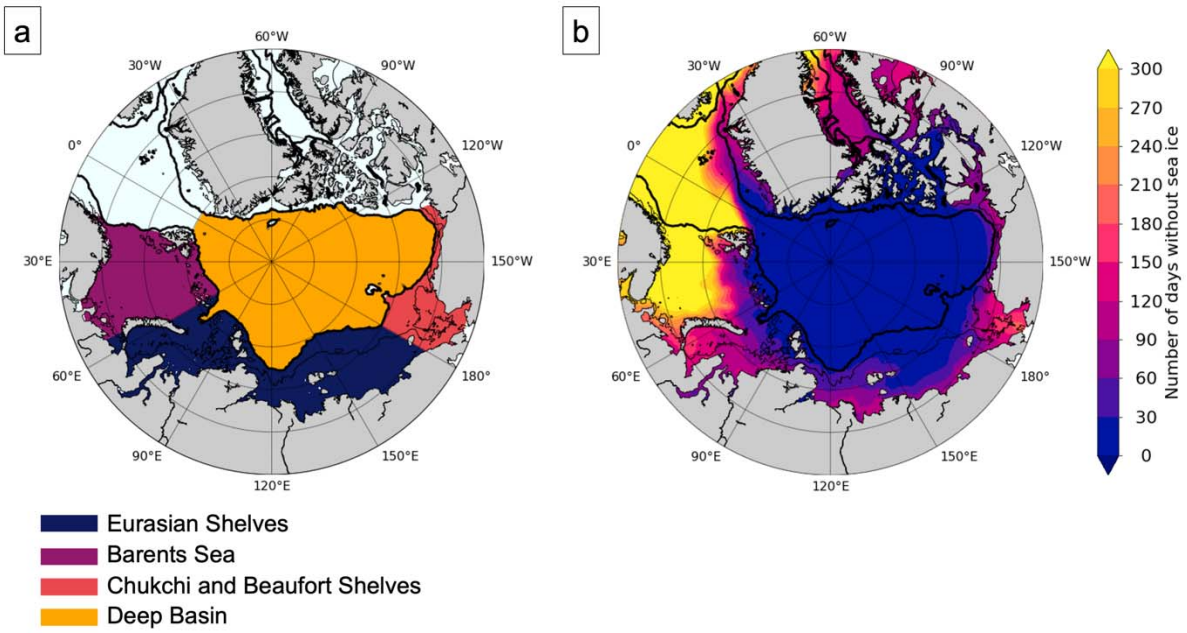

Figure 1. (a) Definitions of the four regions considered in this study; (b) Map of the annual average of the ice-free period duration between 1994 and 2014. Thick black line corresponds to isobath 500 m and thin black line to isobath 50 m.

3 Seasonal Variability of Sea-Ice Conditions, Mixed Layer Depth and Salinity

We start by computing the average annual duration of the ice-free period at each grid cell over 1994-2014 (Figure 1b). The Barents Sea is characterized by the strong influence of an inflow of warm Atlantic Water that prevents the formation of sea ice throughout the year (Arthun et al., 2012). On average, the seasonal ice zone (defined as the area partially covered by sea ice during the year) represents 60% of the Barents Sea surface while 28% is permanently sea ice free and only 12% of the surface is permanently sea ice covered. Overall, the spatial pattern of the sea ice conditions in the Barents Sea (Figure 2a, b, c and d, and Figure 3) is coherent with observations and is likely driven by the influence of Atlantic Water and sea ice import in this area (Lind et al., 2018; Barton et al., 2022). Similarly, the Eurasian Shelves and the Chukchi and Beaufort Shelves are mainly occupied by the seasonal ice zone (64% and 73% respectively). In contrast, most of the deep Basin is characterized by a perennial ice zone (92%), with a thicker ice all year long without much seasonal variability (Figure 2a, b, c and d and Figure 3).

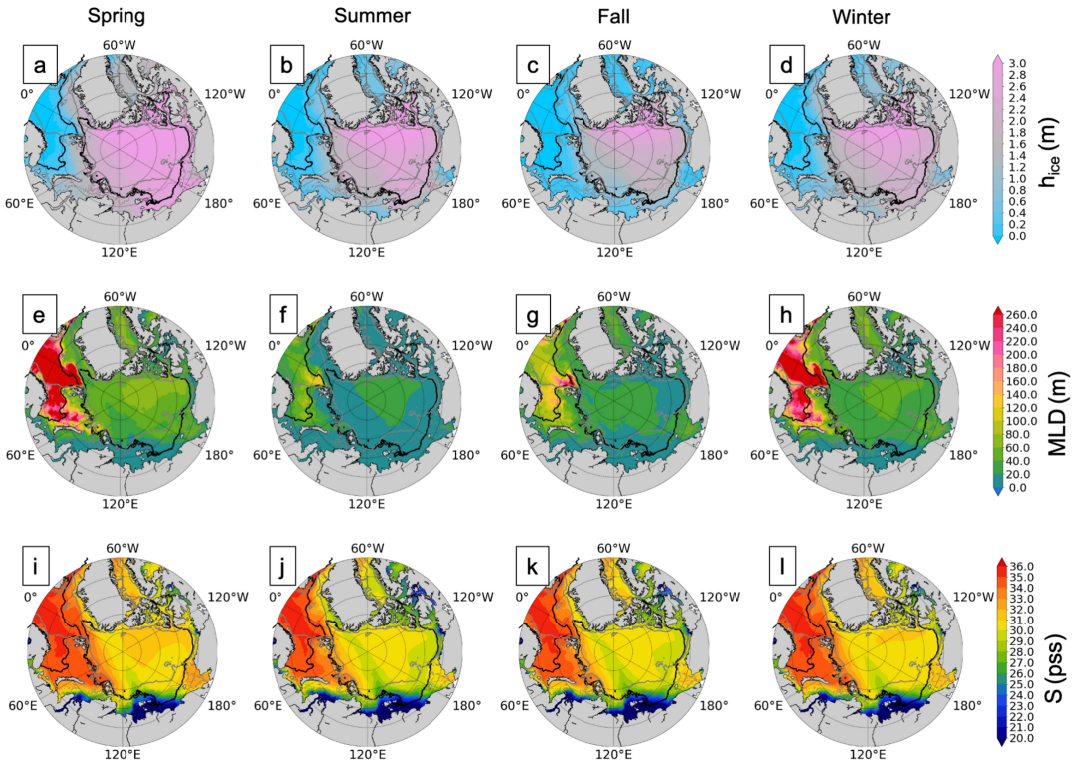

Figure 2. For the period between 1994 and 2014, seasonal average (over the period 1994-2014) of sea ice thickness (a-d), mixed layer depth (e-h) and mixed layer salinity (i-j) for spring (March, April, May – a, e, i), summer (June, July, August – b, f, j), fall (September, October, November – c, g, k) and winter (December, January, February – d, h, l). The black lines correspond to the transitions between the no-ice zone, the seasonal ice zone and the perennial ice zone. The thick gray line corresponds to isobath 500 m and thin gray line to isobath 50 m.

The Barents Sea exhibits the deepest MLD (below 150 m on average in Winter and Spring; Figure 3), with deeper MLD in the ice-free parts of the Barents Sea (Figure 2 e, f, g and h), which is consistent with the observed spatial pattern of MLD (Peralta-Ferriz and Woodgate, 2015). Over the Eurasian Shelves and the Chukchi and Beaufort Shelves, the MLD seasonal variability is limited by the shallow bathymetry and thus the MLD does not exceed 40 m (Figure 3b and c). In the Deep Basin, the MLD reaches deeper values on average than over the Eurasian Shelves and the Chukchi and Beaufort Shelves but remains shallower than in the Barents Sea (Figure 3d). Here again, the model MLD are in close agreement with the observations reported by Peralta-Ferriz and Woodgate (2015), with a seasonal variability between 5 m and 50 m.

We then examine the seasonal variations in MLS. Over the Arctic shelves there are large spatial variations in MLS (Figure 2i, j k and l). In the Barents Sea, the MLS is characterized by the presence of a polar front between the Atlantic and Arctic water (Lind et al., 2018), and varies seasonally between 33.5 pss and 34.5 pss. In this region, the MLS spatial pattern exhibits the signature of the salty Atlantic water inflow close to the SIE (Oziel et al, 2016). The MLS in Chukchi Shelf is also relatively high (between 28.5 pss and 31.5 pss on average; Figure 3c), which is due to the advection of Pacific water from the Bering Strait (Woodgate et al., 2012; Aksenov et al., 2016). In contrast, the MLS in the Beaufort and Eurasian shelves is rather low. These regions are feed by large river runoff that results in low MLS over large parts of the shelf (e.g. the Mackenzie in the Beaufort shelf, the Ob and the Yenisey in the Kara Sea and the Lena in the Laptev Sea). Over the Eurasian Shelves, the average MLS varies between 24.8 pss and 27.2 pss (Figure 3b). The lowest MLS values are visible in the seasonal ice zone, which also corresponds to areas close from the coast, and thus under the influence of rivers runoff. In contrast to the shelves, the MLS in the Deep Basin exhibits smaller spatial and seasonal variability (evolving between 29.5 pss and 31 pss during the year; Figure 3d), with higher MLS in the Eurasian side than in the Canadian Basin and the Beaufort Gyre.

Despite some regional differences, all region exhibits a similar timing of the seasonal variations of the different quantities considered here (Figure 3), that align well with the seasonal cycle obtained from observations by Peralta-Ferriz and Woodgate (2015). During Spring, MLS and the sea ice thickness increase while the MLD reaches its maximum and starts to decrease at the end of the period. The summer period corresponds to a quick and strong decrease in MLD,

MLS and sea ice thickness. During fall and winter, while the sea ice thickness increases, the MLS increases and the MLD deepening slows down.

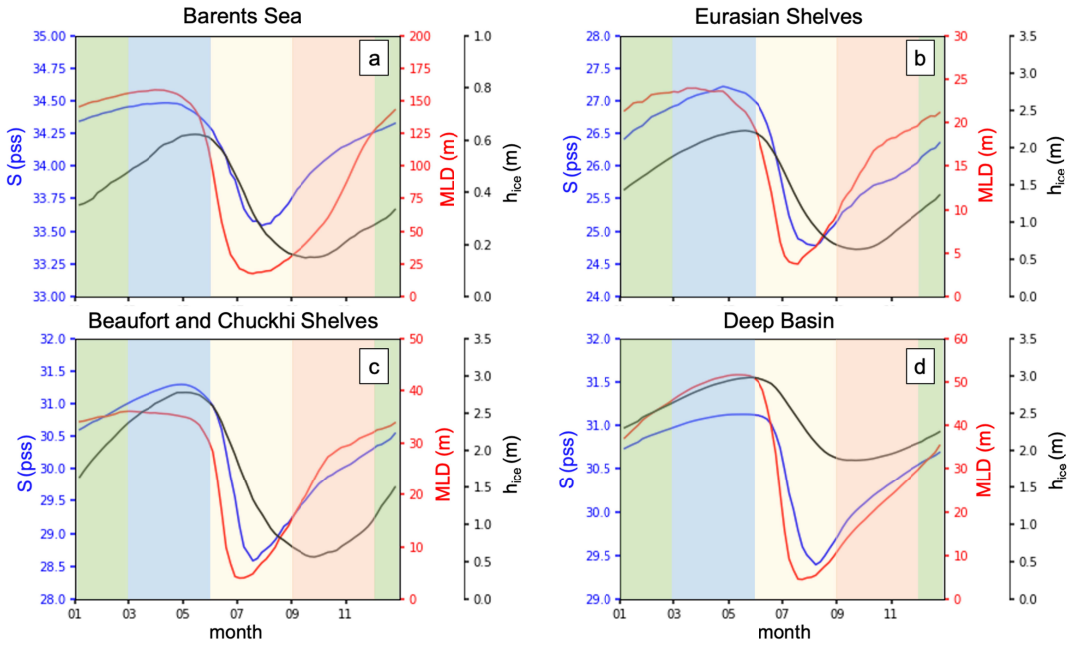

Figure 3. Average seasonal cycle (over the period 1994-2014) of the sea ice thickness (black), mixed layer salinity (blue) and mixed layer depth (red) for the four regions shown in Figure 1a: the Barents Sea (a), the Eurasian Shelves(b), the Beaufort and Chukchi Shelves (c) and the Deep Basin (d). The change of background color corresponds to the different seasons.

4 Seasonal budget of the Mixed Layer Salinity

We then estimate the full MLS budget from Eq. (1). Results are shown as maps for each season (Figures 4, 5, 6, 7) and as time series for the four regions of interest (Figure 8).

During Spring, the MLS tends to increase slightly on average, with the largest increased localized in the seasonal ice zone and over the shelves (Figure 4 and 8). This positive $\partial_t S$ results from the sea ice freezing and the vertical flux, associated with a deepening of the mixed layer. The largest salinity increase is visible in the vicinity of the river mouths in the Eurasian Shelves and the Chukchi and Beaufort Shelves, with values of $\partial_t S$ values between 0.1 pss month^{-1} and 0.3 pss month^{-1}. In contrast, the horizontal flux results in negative $\partial_t S$ over most of the shelves. In addition to the overall positive $\partial_t S$, some negative spots of $\partial_t S$ are seen in some regions along the coasts of the Barents Sea and the Eurasian Shelves (due to riverine water advection and

negative vertical fluxes) and along the Greenland Shelf (due to sea ice melting and negative vertical fluxes). Some of these areas of negative $\partial_t \boldsymbol{S}$ also exhibit a negative contribution from the vertical flux.

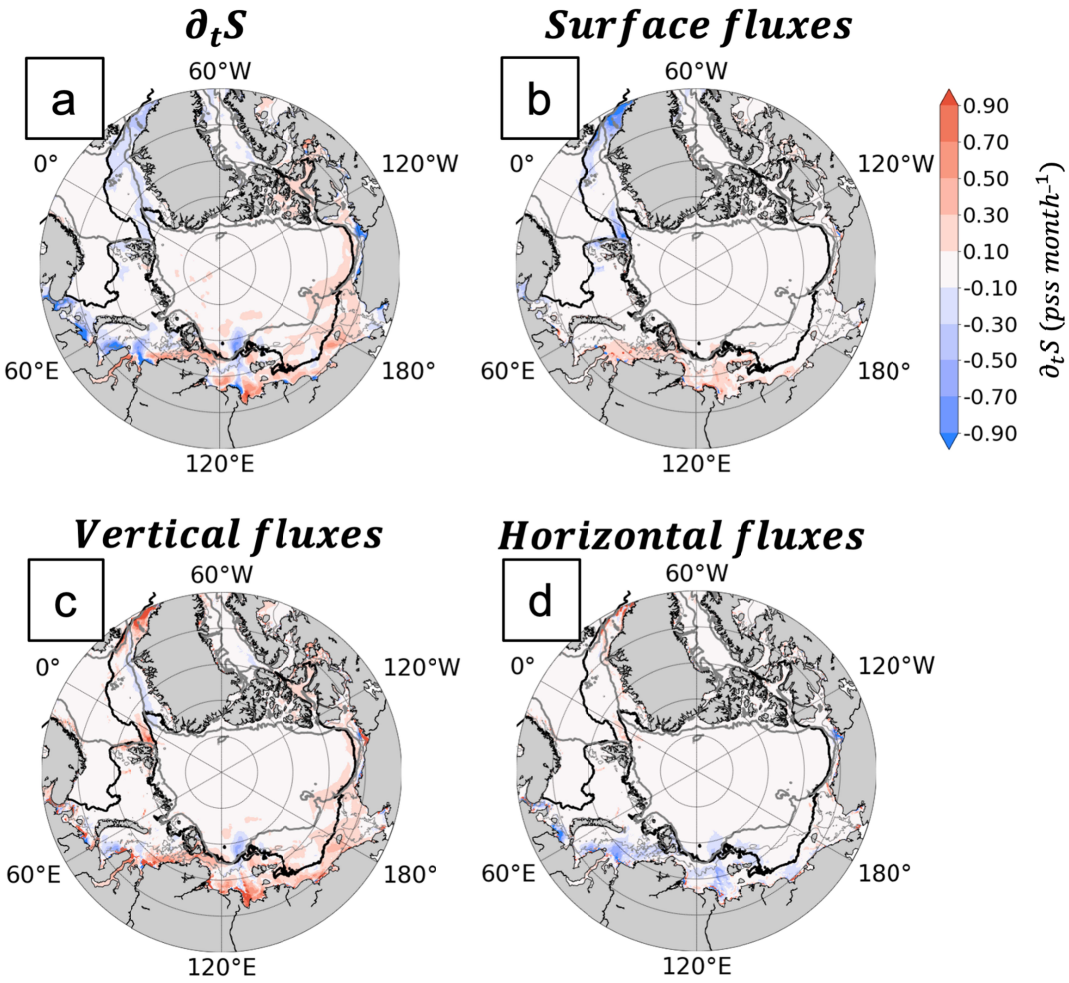

Figure 4. Maps of the different contribution to mixed layer salinity budget in spring, mixed layer salinity budget: (a) salinity change ($\partial_t S$); (b) surface flux; (c) vertical flux; (d) horizontal flux. The black lines correspond to the transitions between the no-ice zone, the seasonal ice zone and the perennial ice zone. The thick gray line corresponds to isobath 500 m and thin gray line to isobath 50 m.

In summer, the main pattern is a decrease in MLS, with a negative value around -1 pss month^{-1} (Figure 5). This decrease in MLS arises from large surface and vertical fluxes that partly compensate each other. This is particularly true over the shelves where the surface and vertical fluxes exceed locally -3 pss month^{-1} and 2 pss month^{-1}, respectively (Figure 8b and c). The largest amplitude of surface and vertical fluxes is found in the Kara and the Chukchi Sea, and

over the Baffin Bay and the Greenland Shelf. Figure 8 also suggest that the summer can indeed be divided into two phases: (i) a fast shoaling until July or mid-July, when the amplitude of the MLS change induced by the sea ice melting is larger than this due to the vertical flux, resulting in a negative $\partial_t S$; and (ii) a slow deepening of the MLD associated with a MLS increase, when vertical mixing prevails over the impact of the sea ice melt, that occurs until fall. For example, in the Chukchi and the Beaufort Sea, the average freshening reaches first its minimum of -2 pss month^{-1} and then increases again to roughly to 0.6 pss month^{-1} for a few months.

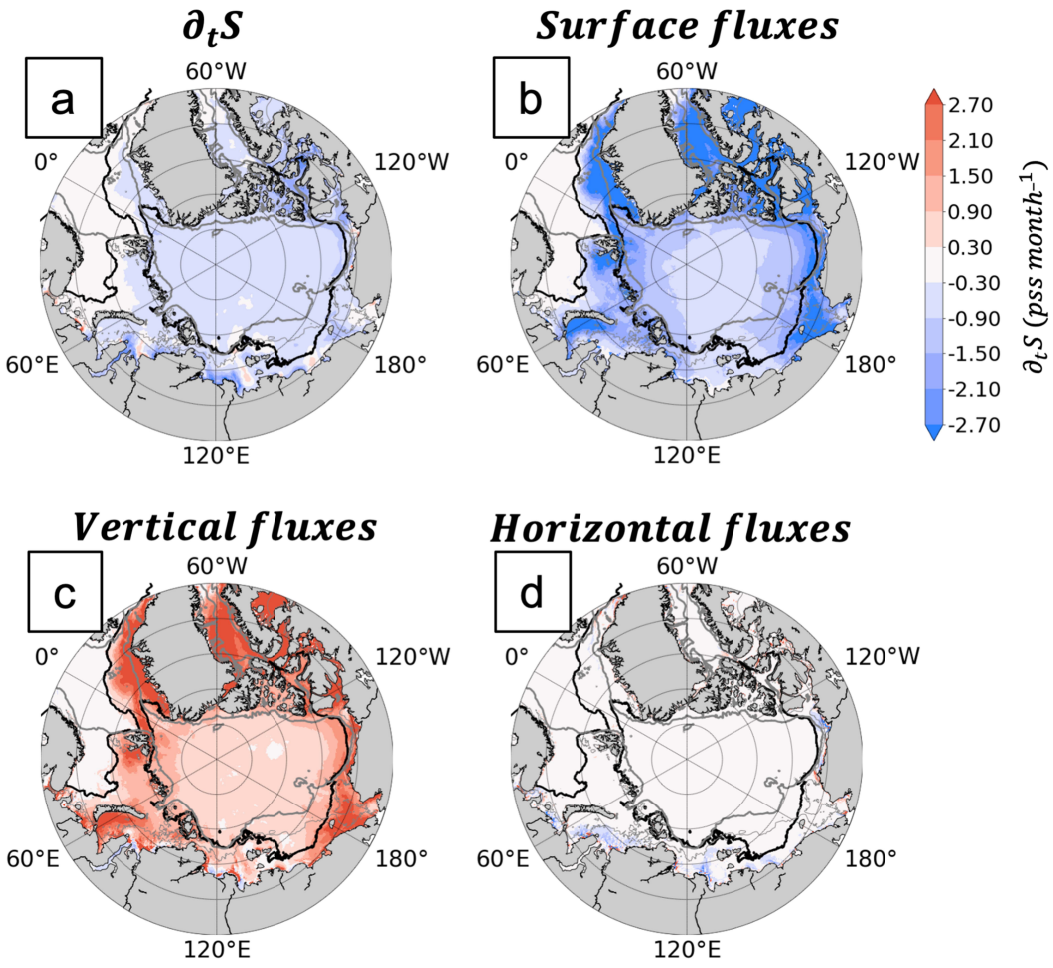

Figure 5. Same as Figure 4 but for summer. Note the different colorbar used here.

During fall, the sea ice melt halts and the MLS tend to increase primarily because of the entrainment of saltier water from underneath (Figure 6). The contribution of the vertical flux strongly changes from the start to the end of fall. In the Eurasian Shelves and the Beaufort and the Chukchi Shelves, this contribution decreases from approximately 1.2 pss month^{-1} to 0.3 pss

266 month^{-1} (Figure 8). Over the Eurasian Shelves, the surface flux associated with brine rejection as
267 sea ice forms also contributes to the MLS increase in the vicinity of the river mouths, but this
268 effect is counterbalanced largely by the negative contribution from the horizontal flux, due to
269 advection of riverine waters. Near Fram Strait, and in the Chukchi Sea, where sea ice melts
270 during this period, the MLS increase remains rather small. In the Eurasian Shelves, brine
271 rejection induces the largest MLS increase. On average, the Chukchi and the Beaufort Shelves
272 exhibit the largest MLS increase, with trends close from 3 pss month^{-1} over large areas.

273

274

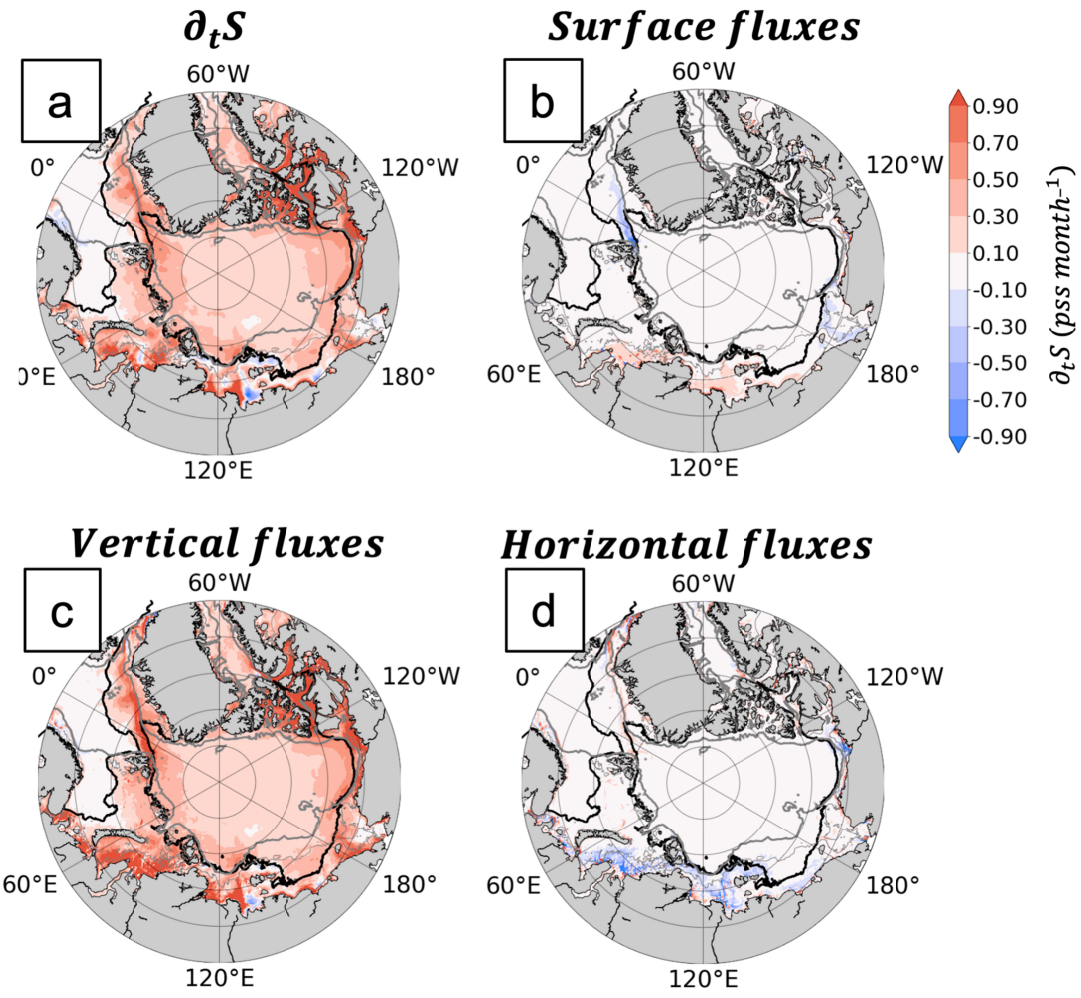

275

276 **Figure 6**. Same as Figure 4 but for fall.

During winter, the main balance for the MLS budget is largely similar to the balance found for Fall, with a decrease of MLS caused by the vertical processes, although the values are overall weaker (around 0.2 pss month^{-1}), especially in the interior of the Arctic basin (Figures 7 and 8). During this period, the relative effect of freezing on MLS becomes stronger. The Eurasian Shelves are a hotspot for the surface flux induced by sea ice freezing, but there the change is MLS is partly compensated by horizontal processes.

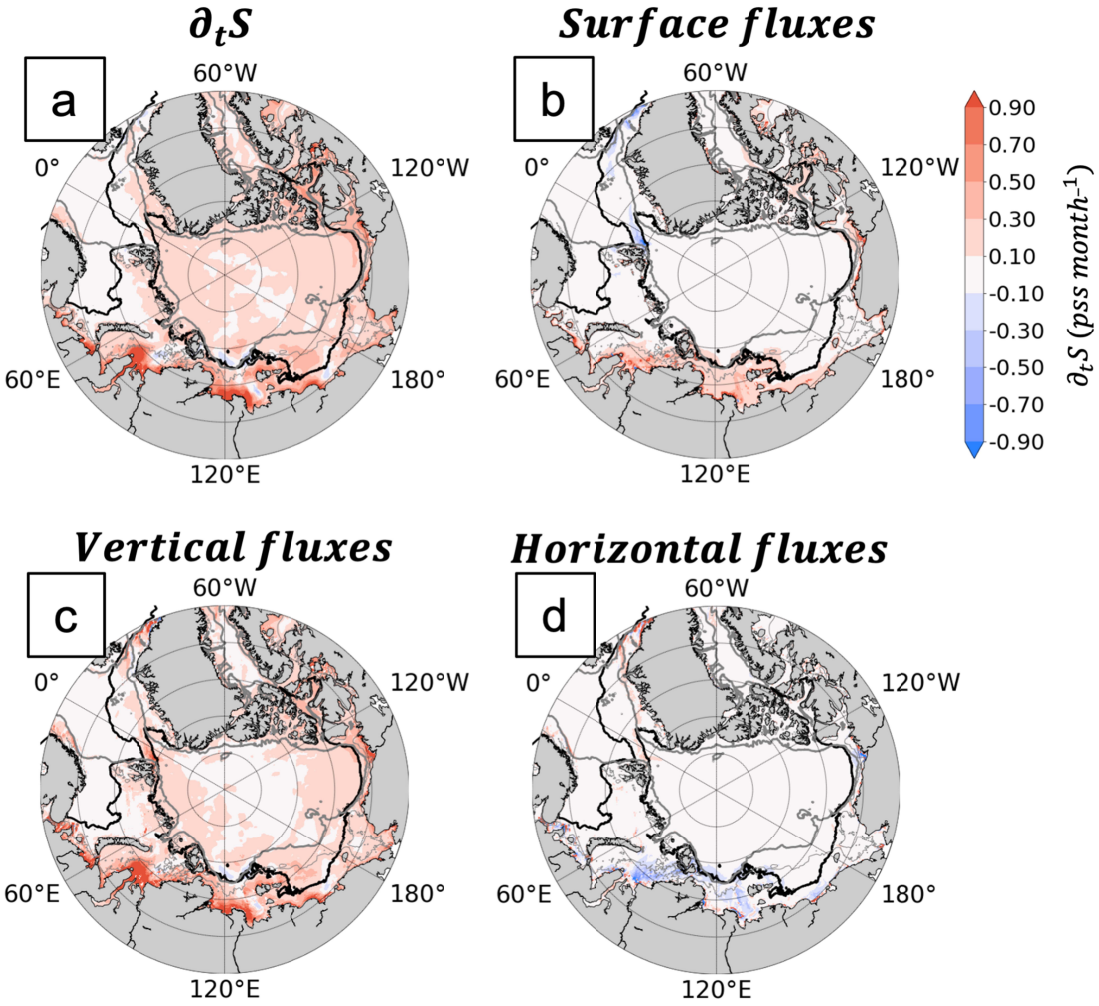

Figure 7. Same as Figure 4 but for winter.

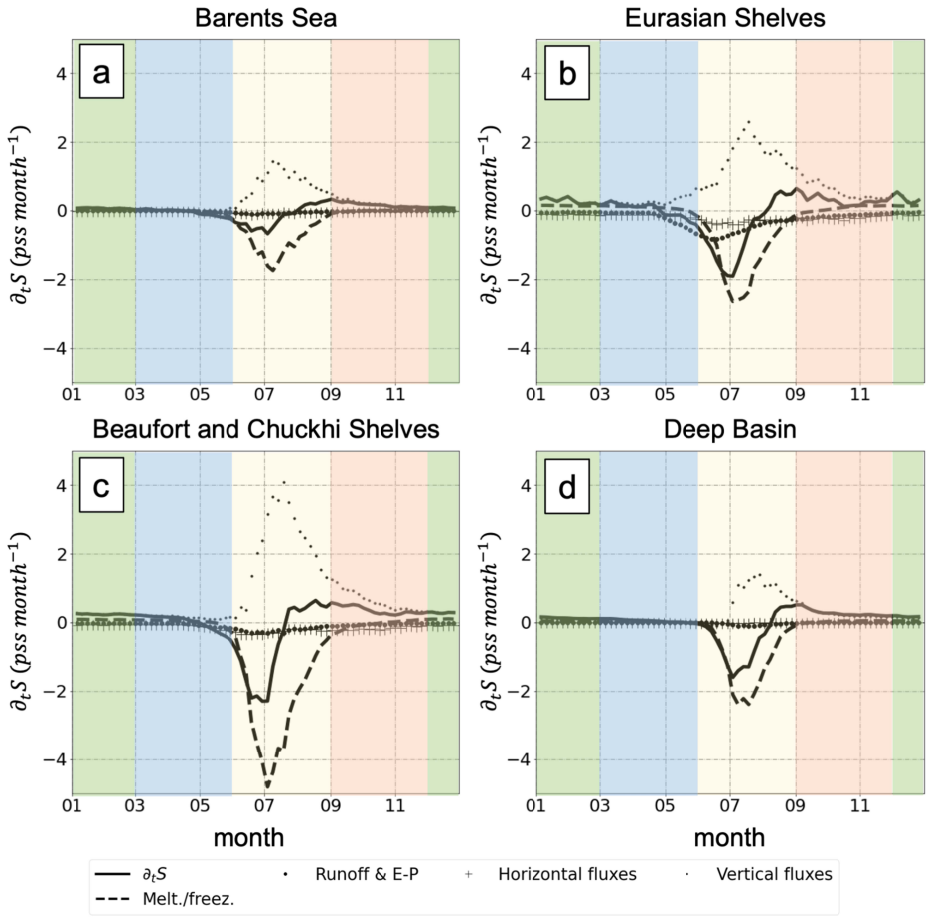

Figure 8. Average seasonal cycle (over the period 1994-2014) of the mixed layer salinity budget for the four regions shown in Figure 1a: the Barents Sea (a), the Eurasian Shelves (b), the Beaufort and Chukchi Shelves (c) and the Deep Basin (d). The change of background color corresponds to the different seasons.

5 Mixed Layer Salinity dynamics at the Sea Ice Edge

In this section, we focus on the MLS budget in the vicinity of the SIE, which is defined as the 15% concentration contour. To that aim each grid point of the model output is characterized by its distance from the closest grid point with sea ice concentration larger (lower) than 15% if the sea ice concentration of this grid point is lower (larger) than 15%. Figure 9 shows the MLS budget per season as a function of the distance from the SIE. During spring (figure 9a), the vicinity of the SIE (50km on both sides) is characterized by a decrease in MLS. There, the MLS change induced by both sea ice melt and river runoff seems explain fully the amplitude of $\partial_t S$, in

spite of a strong and relatively persistent vertical flux that tend to oppose to the freshening. Note that, at this early time of the melting season, river runoff plays a major role, contributing up to -0.5 pss month^{-1} . This is because at this time of the year, the SIE is still found close to the coast in many regions, and especially over the Eurasian Shelves. Under the sea ice, when the distance from the SIE increases, the sea ice melt contribution gradually reduces while the horizontal fluxes contribution to the freshening increases. During this period, the mixed layer is relatively deep (Figure 9e), with deeper mixed layer found in the ice-free area (between 250 m and 400 m on average) than under sea ice (between 100 m and 200 m). In reality, the ice-free regions during that period correspond to the regions that are ice-free all year long.

During summer, the mixed layer is the shallowest (less than 30 m), especially at the SIE where is remains above 5 m (Figure 9b). The shallow mixed layers results from the large ice melt flux (up to - 4pss month^{-1} ; Figure 9b) that tend to stratify the upper ocean layer. This makes the mixed layer particularly sensitive to changes induced by surface and vertical fluxes. Interestingly, $\partial_t S$ change its sign at the SIE: under sea ice, the mixed layer is getting fresher while in free ice regions the mixed layer gets saltier. This is explained by the dominance of melting in the sea ice covered region while vertical mixing (between 1 and 5 pss month^{-1}) is dominant in the ice free region, where the melt ceases as sea ice retreats. In this region, the mixed layer deepens, and the MLS increases as the distance from the SIE increases, in response to the contribution from the vertical flux (Figure 9b). Once again, the strongest flux is shown within +/-50 km from the moving SIE. During Summer, the contribution from the horizontal flux is stronger in the ice-free area where the river runoff counterbalances the MLS increase.

During fall, $\partial_t S$ is positive everywhere, due to the end of the melting season and the start of freezing (Figure 9c). Also, the amplitudes of $\partial_t S$ absolute value are twice smaller than during summer. While $\partial_t S$ amplitude exceeds 1 pss month^{-1} on both side of the SIE, the maximum $\partial_t S$ amplitude only reaches 0.5 pss month^{-1} at the SIE in fall. Indeed, on both sides of the SIE, the contribution from the vertical flux is the main driver of the salinity increase and is again intensified closer to the SIE. In the sea ice free region, the horizontal advection of freshwater from river runoff induces a negative $\partial_t S$ on both sides of the SIE, albeit with a smaller amplitude.

Finally, in winter, MLS and MLD increase close to SIE (Figure 9d and e). The mixed layer reaches its deepest annual value and exceeds 100 m under sea ice and 400 m in the free ice region. The average is largely biased by the deep mixed layer depth found in the ice-free Barents Sea during winter. $\partial_t S$ is mainly explained by freezing (under sea ice) and the vertical flux, although its amplitude is lower than during the other seasons (reaching only 0.1 pss month^{-1} at more than 150 km of the SIE under the sea ice). Interestingly, in contrast to the other seasons, during winter, the processes responsible for the vertical flux are likely involving both brine rejection under the ice, and deep convection occurring in Barents Sea ice free region.

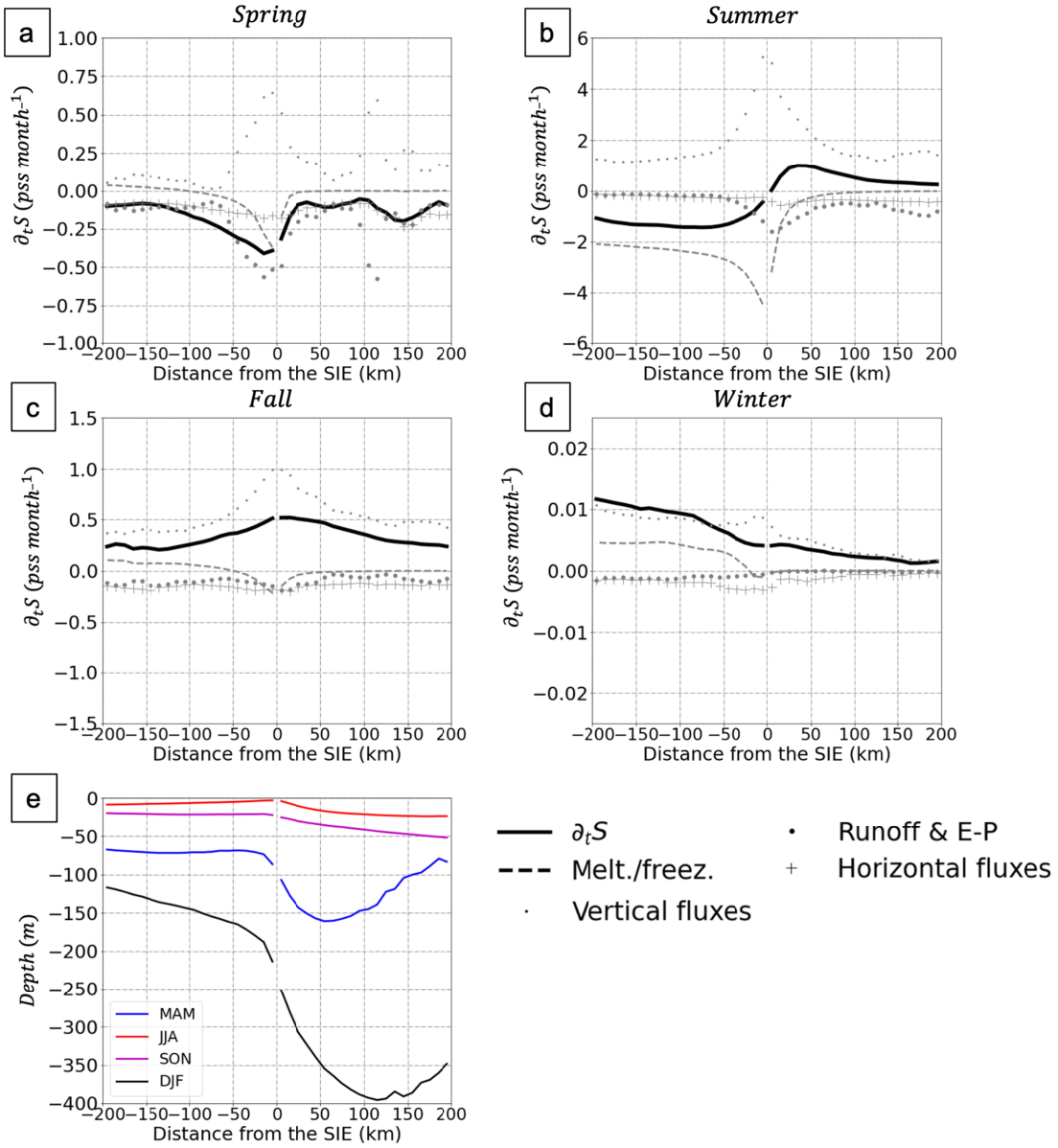

Figure 9. Mean seasonal mixed Layer Salinity budget as a function of distance from the sea ice edge (SIE) during spring (a), summer (b), fall (c) and winter (d). Mean seasonal spatial variations of the mixed layer depth as a function of distance from the sea ice edge. Positive distances from the sea ice edge correspond to ice-free areas and negative distances corresponds to ice-covered areas.

6 Discussion and Conclusion

The Arctic Ocean is characterized by an expanding seasonal ice zone, where the large seasonal variations of the sea ice conditions influence the seasonal variability of the mixed layer, and in particular its salinity. Based on a salinity budget in the mixed layer applied to the outputs of a high-resolution ocean-sea ice model, we have found that on average, there is a seasonal balance between the contribution to the change in mixed layer salinity of sea ice freezing/melting and the vertical flux at the base of the Arctic Ocean mixed layer. It is interesting to note that, although the amounts of freshwater brought to the ocean surface by sea ice freezing and melting are roughly of equal amplitudes, their impacts on the mixed layer salinity are fundamentally asymmetric over a seasonal cycle. Indeed, the melt-induced freshwater flux, which is large during a short period of time during summer, tends to create a thin stratified upper layer. In contrast, the negative flux from sea ice brine rejection is smaller but sustained over a longer period, when the mixed layer is also deeper. The vertical processes (mixing and entrainment) also play a different role depending on the season and region considered. In regions where sea ice retreats, the vertical mixing tends to be the dominant forcing to erase the surface freshening. In contrast, during winter, the vertical processes are playing a large role as they result from brine rejection under the ice and deep convection in the ice-free region of the Barents Sea. In some specific regions, mainly over shelves, advection and river runoff also contribute to redistribute freshwater to the mixed layer.

A striking result of our study is that the mixed layer salinity change and flux are generally largely intensified within the 50 km of the sea ice edge, making the sea ice edge a hot spot for the seasonal variability. There, the sea-ice induced surface fluxes are intensified and largely counterbalanced by strong vertical processes (similar to what was observed by Dewey et al. (2017) in the Canadian). In addition, we also found that over the shelves and in the vicinity of river discharge areas, horizontal fluxes and riverine freshwater more strongly impact mixed layer salinity budget close to the sea ice edge, affecting the whole mixed layer salinity budget at the scale of the shelves.

In our investigation we have considers the different regions independently. Yet it is clear that the connectivity between the regions is also key to better understanding the Arctic Ocean evolution. While at first order the seasonal processes driving the mixed layer evolution contributes to the halocline formation, the connections between the shelves and the deep basins are also a key player of the formation of this barrier layer which limits the upward diffusion of Atlantic waters heat toward the surface (Rudels et al, 1996). The connections between the shelves and the deep basins also participate to the halocline formation through an advective mode: melting of advected sea ice formed at the surface of the shelves and cascading of dense water formed on the shelves during sea ice formation supply the Arctic halocline. The key aspect of this connectivity is enhanced by the increase of dense water cascading when the shelves are seasonally ice-covered (Luneva et al., 2020). Conversely, these shelf/basin exchanges also influence the trend and interannual mixed layer salinity variability, by conveying the changes of salinity below the mixed layer to the mixed layer through vertical entrainment. The expansion of the seasonal ice zone to the deep basins will likely results in large changes the seasonal cycle of the mixed layer properties. Such changes should be considered and quantified in future studies.

Acknowledgment

AS acknowledges the support of a CNES Postdoctoral fellowship and the support of European Space Agency Climate Change Initiative CCI + SSS project. CL and CT were supported by the project MEDLEY funded by JPI Climate and JPI Oceans, under the agreement ANR-19- JPOC-000. This work is a contribution to the TOSCA/SMOS-Ocean project supported by CNES. The pan-Arctic simulation was performed using HPC resources from the French GENCI-CINES center (Grant 2018-A0050107420).

Open research

Data Availability Statement

399 Version 1.1 of the CREG12. L75-REF08 Canadian Regional model based on NEMO used for
400 producing the model output is available in open access at
401 https://doi.org/10.5281/zenodo.5789520. It includes the configuration files, the links to boundary
402 conditions, atmospheric forcing and initialization files.

403

404 **References**

405 Aagaard, K., Coachman, L. K., & Carmack, E. (1981). On the halocline of the Arctic Ocean.
406 Deep Sea Research Part A. Oceanographic Research Papers, 28(6), 529-545.

407 Aksenov, Y., Karcher, M., Proshutinsky, A., Gerdes, R., De Cuevas, B., Golubeva, E., ... &
408 Nurser, A. G. (2016). Arctic pathways of Pacific Water: Arctic Ocean Model Intercomparison
409 experiments. Journal of Geophysical Research: Oceans, 121(1), 27-59.

410 Årthun, M., Onarheim, I. H., Dörr, J., & Eldevik, T. (2021). The seasonal and regional transition
411 to an ice-free Arctic. Geophysical Research Letters, 48(1), e2020GL090825.

412 Barton, B. I., Lique, C., Lenn, Y. D., & Talandier, C. (2022). An ice-ocean model study of the
413 mid-2000s regime change in the Barents Sea. Journal of Geophysical Research: Oceans, 127(11),
414 e2021JC018280.

415 Bauch, D., Hoelemann, J. A., Nikulina, A., Wegner, C., Janout, M. A., Timokhov, L. A., &
416 Kassens, H. (2013). Correlation of river water and local sea-ice melting on the Laptev Sea shelf
417 (Siberian Arctic). Journal of Geophysical Research: Oceans, 118(1), 550-561.

418 Carmack, E. C. (2007). The alpha/beta ocean distinction: A perspective on freshwater fluxes,
419 convection, nutrients and productivity in high-latitude seas. Deep Sea Research Part II: Topical
420 Studies in Oceanography, 54(23-26), 2578-2598.

421 Crews, L., Lee, C. M., Rainville, L., & Thomson, J. (2022). Direct Observations of the Role of
422 Lateral Advection of Sea Ice Meltwater in the Onset of Autumn Freeze Up. Journal of
423 Geophysical Research: Oceans, 127(2), e2021JC017775.

424 Dewey, S. R., Morison, J. H., & Zhang, J. (2017). An edge-referenced surface fresh layer in the
425 Beaufort Sea seasonal ice zone. Journal of Physical Oceanography, 47(5), 1125-1144.

426 Haine, T. W., & Martin, T. (2017). The Arctic-Subarctic sea ice system is entering a seasonal

regime: Implications for future Arctic amplification. Scientific Reports, 7(1), 1-9.

Hu, X., P. G. Myers, and Y. Lu, 2019: Pacific water pathway in the Arctic Ocean and Beaufort Gyre in two simulations with dif- ferent horizontal resolutions. J. Geophys. Res. Oceans, 124, 6414–6432, https://doi.org/10.1029/2019JC015111.

Jackson, J. M., Williams, W. J., & Carmack, E. C. (2012). Winter sea-ice melt in the Canada Basin, Arctic Ocean. Geophysical Research Letters, 39(3).

Janout, M., Hölemann, J., Juhls, B., Krumpen, T., Rabe, B., Bauch, D., ... & Timokhov, L. (2016). Episodic warming of near-bottom waters under the Arctic sea ice on the central Laptev Sea shelf. Geophysical Research Letters, 43(1), 264-272.

Johnson, G. C., Schmidtko, S., & Lyman, J. M. (2012). Relative contributions of temperature and salinity to seasonal mixed layer density changes and horizontal density gradients. Journal of Geophysical Research: Oceans, 117(C4).

Kacimi, S., & Kwok, R. (2022). Arctic Snow Depth, Ice Thickness, and Volume From ICESat-2 and CryoSat-2: 2018–2021. Geophysical Research Letters, 49(5), e2021GL097448.

Kawaguchi, Y., Kikuchi, T., & Inoue, R. (2014). Vertical heat transfer based on direct microstructure measurements in the ice-free Pacific-side Arctic Ocean: the role and impact of the Pacific water intrusion. Journal of oceanography, 70, 343-353.

Kinnard, C., Zdanowicz, C. M., Koerner, R. M., & Fisher, D. A. (2008). A changing Arctic seasonal ice zone: Observations from 1870–2003 and possible oceanographic consequences. Geophysical Research Letters, 35(2).

Kolodziejczyk, N., & Gaillard, F. (2013). Variability of the heat and salt budget in the subtropical southeastern Pacific mixed layer between 2004 and 2010: Spice injection mechanism. Journal of physical oceanography, 43(9), 1880-1898.

Kwok, R. (2018). Arctic sea ice thickness, volume, and multiyear ice coverage: losses and coupled variability (1958–2018). Environmental Research Letters, 13(10), 105005.

Lemke, P., & Manley, T. O. (1984). The seasonal variation of the mixed layer and the pycnocline under polar sea ice. Journal of Geophysical Research: Oceans, 89(C4), 6494-6504.

Lind, S., Ingvaldsen, R. B., & Furevik, T. (2018). Arctic warming hotspot in the northern

455 Barents Sea linked to declining sea-ice import. Nature climate change, 8(7), 634-639.

456 Luneva, M. V., Ivanov, V. V., Tuzov, F., Aksenov, Y., Harle, J. D., Kelly, S., & Holt, J. T.
457 (2020). Hotspots of dense water cascading in the Arctic Ocean: Implications for the Pacific water
458 pathways. Journal of Geophysical Research: Oceans, 125(10), e2020JC016044.

459 Madec, G., Bourdallé-Badie, R., Bouttier, P. A., Bricaud, C., Bruciaferri, D., Calvert, D., ... &
460 Vancoppenolle, M. (2017). NEMO ocean engine.

461 Manucharyan, G. E., & Thompson, A. F. (2017). Submesoscale sea ice-ocean interactions in
462 marginal ice zones. Journal of Geophysical Research: Oceans, 122(12), 9455-9475.

463 Macdonald, R. W., Carmack, E. C., McLaughlin, F. A., Falkner, K. K., & Swift, J. H. (1999).
464 Connections among ice, runoff and atmospheric forcing in the Beaufort Gyre. Geophysical
465 Research Letters, 26(15), 2223-2226.

466 Meneghello, G., Marshall, J., Lique, C., Isachsen, P. E., Doddridge, E., Campin, J. M., ... &
467 Talandier, C. (2021). Genesis and decay of mesoscale baroclinic eddies in the seasonally ice-
468 covered interior Arctic Ocean. Journal of Physical Oceanography, 51(1), 115-129.

469 Moisan, John R., and Pearn P. Niiler. "The seasonal heat budget of the North Pacific: Net heat
470 flux and heat storage rates (1950–1990)." Journal of Physical Oceanography 28.3 (1998): 401-
471 421.

472 Mulligan, R. P., & Perrie, W. (2019). Circulation and structure of the Mackenzie River plume in
473 the coastal Arctic Ocean. Continental Shelf Research, 177, 59-68.

474 Notz, D. (2009). The future of ice sheets and sea ice: Between reversible retreat and unstoppable
475 loss. Proceedings of the National Academy of Sciences, 106(49), 20590-20595.

476 Nurser, A. J. G., & Bacon, S. (2014). The rossby radius in the Arctic Ocean. Ocean Science,
477 10(6), 967-975.

478 Oziel, L., Sirven, J., & Gascard, J. C. (2016). The Barents Sea frontal zones and water masses
479 variability (1980–2011). Ocean Science, 12(1), 169-184.

480 Pellichero, V., Sallée, J. B., Schmidtko, S., Roquet, F., & Charrassin, J. B. (2017). The ocean
481 mixed layer under Southern Ocean sea-ice: Seasonal cycle and forcing. Journal of Geophysical
482 Research: Oceans, 122(2), 1608-1633.

Peralta-Ferriz, C., & Woodgate, R. A. (2015). Seasonal and interannual variability of pan-Arctic surface mixed layer properties from 1979 to 2012 from hydrographic data, and the dominance of stratification for multiyear mixed layer depth shoaling. Progress in Oceanography, 134, 19-53.

Polyakov, I. V., Alkire, M. B., Bluhm, B. A., Brown, K. A., Carmack, E. C., Chierici, M., ... & Wassmann, P. (2020). Borealization of the Arctic Ocean in response to anomalous advection from sub-Arctic seas. Frontiers in Marine Science, 7, 491.

Proshutinsky, A., Krishfield, R., Timmermans, M. L., Toole, J., Carmack, E., McLaughlin, F., ... & Shimada, K. (2009). Beaufort Gyre freshwater reservoir: State and variability from observations. Journal of Geophysical Research: Oceans, 114(C1).

Rainville, L., Lee, C. M., & Woodgate, R. A. (2011). Impact of wind-driven mixing in the Arctic Ocean. Oceanography, 24(3), 136-145.

Regan, H. C., Lique, C., & Armitage, T. W. (2019). The Beaufort Gyre extent, shape, and location between 2003 and 2014 from satellite observations. Journal of Geophysical Research: Oceans, 124(2), 844-862.

Regan, H., Lique, C., Talandier, C., & Meneghello, G. (2020). Response of total and eddy kinetic energy to the recent spinup of the Beaufort Gyre. Journal of Physical Oceanography, 50(3), 575-594.

Ren, L., Speer, K., & Chassignet, E. P. (2011). The mixed layer salinity budget and sea ice in the Southern Ocean. Journal of Geophysical Research: Oceans, 116(C8).

Rippeth, T., & Fine, E. (2022). Turbulent mixing in a changing Arctic Ocean. Oceanography.

Rudels, B., Anderson, L. G., & Jones, E. P. (1996). Formation and evolution of the surface mixed layer and halocline of the Arctic Ocean. Journal of Geophysical Research: Oceans, 101(C4), 8807-8821.

Rudels, B., and E. Carmack. (2022). Arctic ocean water mass structure and circulation. Oceanography 35(3–4):52–65, https://doi.org/10.5670/oceanog.2022.116.

Rousset, C., Vancoppenolle, M., Madec, G., Fichefet, T., Flavoni, S., Barthélemy, A., ... & Vivier, F. (2015). The Louvain-La-Neuve sea ice model LIM3. 6: global and regional capabilities. Geoscientific Model Development, 8(10), 2991-3005.

Smith, M., Stammerjohn, S., Persson, O., Rainville, L., Liu, G., Perrie, W., ... & Thomson, J.

(2018). Episodic reversal of autumn ice advance caused by release of ocean heat in the Beaufort Sea. Journal of Geophysical Research: Oceans, 123(5), 3164-3185.

Steele, M., Ermold, W., & Zhang, J. (2011). Modeling the formation and fate of the near-surface temperature maximum in the Canadian Basin of the Arctic Ocean. Journal of Geophysical Research: Oceans, 116(C11).

Stewart, K. D., & Haine, T. W. (2016). Thermobaricity in the transition zones between alpha and beta oceans. Journal of Physical Oceanography, 46(6), 1805-1821.

Stroeve, J. C., Markus, T., Boisvert, L., Miller, J., & Barrett, A. (2014). Changes in Arctic melt season and implications for sea ice loss. Geophysical Research Letters, 41(4), 1216-1225.

Stroeve, J., & Notz, D. (2018). Changing state of Arctic sea ice across all seasons. Environmental Research Letters, 13(10), 103001.

Talandier, C., & Lique, C. (2021). CREG12.L75-REF08. https://doi.org/10.5281/zenodo.5789520

Tarasenko, A., Supply, A., Kusse-Tiuz, N., Ivanov, V., Makhotin, M., Tournadre, J., ... & Reverdin, G. (2021). Properties of surface water masses in the Laptev and the East Siberian seas in summer 2018 from in situ and satellite data. Ocean Science, 17(1), 221-247.

Timmermans, M. L., Cole, S., & Toole, J. (2012). Horizontal density structure and restratification of the Arctic Ocean surface layer. Journal of Physical Oceanography, 42(4), 659-668.

Timmermans, M. L. (2015). The impact of stored solar heat on Arctic sea ice growth. Geophysical Research Letters, 42(15), 6399-6406.

Treguier, A. M., Deshayes, J., Le Sommer, J., Lique, C., Madec, G., Penduff, T., et al. (2014). Meridional transport of salt in the global ocean from an eddy-resolving model. Ocean Science, 10(2), 243–255. https://doi.org/10.5194/os-10-243-2014

Toole, J. M., Timmermans, M. L., Perovich, D. K., Krishfield, R. A., Proshutinsky, A., & Richter-Menge, J. A. (2010). Influences of the ocean surface mixed layer and thermohaline stratification on Arctic Sea ice in the central Canada Basin. Journal of Geophysical Research: Oceans, 115(C10).

Woodgate, R. A. (2018). Increases in the Pacific inflow to the Arctic from 1990 to 2015, and insights into seasonal trends and driving mechanisms from year-round Bering Strait mooring data. Progress in Oceanography, 160, 124-154.

Yang, J. (2006). The seasonal variability of the Arctic Ocean Ekman transport and its role in the mixed layer heat and salt fluxes. Journal of Climate, 19(20), 5366-5387.